Int J Adv Manuf Technol (2017) 91:1547–1566
DOI 10.1007/s00170-016-9824-5

ORIGINAL ARTICLE

An accuracy design approach for a multi-axis NC machine tool based on reliability theory

Ziling Zhang[1] · **Zhifeng Liu**[1] · **Ligang Cai**[1] · **Qiang Cheng**[1] · **Yin Qi**[2]

Received: 15 May 2016 / Accepted: 21 November 2016 / Published online: 13 December 2016

Abstract Accuracy design constitutes an important role in machine tool designing. It is used to determine the permissible level of each error parameter of a machine tool, so that any criterion can be optimized. Geometric, thermal-induced, and cutting force-induced errors are responsible for a large number of comprehensive errors of a machine tool. These errors not only influence the machining accuracy but are also of great importance for accuracy design to be performed. The aim of this paper is the proposal of a general approach that simultaneously considered geometric, thermal-induced, and cutting force-induced errors, in order for machine tool errors to be allocated. By homogeneous transformation matrix (HTM) application, a comprehensive error model was developed for the machining accuracy of a machine tool to be acquired. In addition, a generalized radial basis function (RBF) neural network modeling method was used in order for a thermal and cutting force-induced error model to be established. Based on the comprehensive error model, the importance sampling method was applied for the reliability and sensitivity analysis of the machine tool to be conducted, and two mathematical models were presented. The first model predicted the reliability of the machine tool, whereas the second was used to identify and optimize the error parameters with larger effect on the reliability. The permissible level of each geometric error parameter can therefore be determined, whereas the reliability met the design requirement and the cost of this machining was optimized. An experiment was conducted on a five-axis machine tool, and the results confirmed the proposed approach being able to display the accuracy design of the machine tool.

Keywords Comprehensive error model · Thermal and cutting force induced error model · Reliability and sensitivity analysis · Accuracy design · Machine tool

Nomenclature

Δx_x	*Positioning error of the X-axis*
Δy_x	*Y direction of straightness error of the X-axis*
Δz_x	*Z direction of straightness error of the X-axis*
$\Delta \alpha_x$	*Roll error of the X-axis*
$\Delta \beta_x$	*Pitch error of the X-axis*
$\Delta \gamma_x$	*Yaw error of the X-axis*
Δx_y	*X direction of straightness error of the Y-axis*
Δy_y	*Positioning error of the Y-axis*
Δz_y	*Z direction of straightness error of the Y-axis*
$\Delta \alpha_y$	*Pitch error of the Y-axis*
$\Delta \beta_y$	*Roll error of the Y-axis*
$\Delta \gamma_y$	*Yaw error of the Y-axis*
Δx_z	*X direction of straightness error of the Z-axis*
Δy_z	*Y direction of straightness error of the Z-axis*
Δz_z	*Positioning error of the Z-axis*
$\Delta \alpha_z$	*Pitch error of the Z-axis*
$\Delta \beta_z$	*Yaw error of the Z-axis*
$\Delta \gamma_z$	*Roll error of the Z-axis*
Δx_B	*X direction run-out error of the B-axis*
Δy_B	*Y direction run-out error of the B-axis*
Δz_B	*Z direction run-out error of the B-axis*
$\Delta \alpha_B$	*Around the X-axis turning error of the B-axis*
$\Delta \beta_B$	*Turning error of the B-axis*
$\Delta \gamma_B$	*Around the Z-axis turning error of the B-axis*

✉ Zhifeng Liu
lzfbjut@gmail.com; lzf@bjut.edu.cn

[1] Beijing Key Laboratory of Advanced Manufacturing Technology, Beijing University of Technology, 100 Pingleyuan Street, Beijing 100124, China

[2] Yingtan Applied Engineering School, Yingtan, Jiangxi 335200, China

Δx_A *X direction run-out error of the A-axis*
Δy_A *Y direction run-out error of the A-axis*
Δz_A *Z direction run-out error of the A-axis*
$\Delta\alpha_A$ *Turning error of the A-axis*
$\Delta\beta_A$ *Around the Y-axis turning error of the A-axis*
$\Delta\gamma_A$ *Around the Z-axis turning error of the A-axis*
Δx_φ *X direction run-out error of the spindle*
Δy_φ *Y direction run-out error of the spindle*
Δz_φ *Z direction run-out error of the spindle*
$\Delta\alpha_\varphi$ *Around the X-axis turning error of the spindle*
$\Delta\beta_\varphi$ *Around the Y-axis turning error of the spindle*
$\Delta\gamma_\varphi$ *Turning error of the spindle*
$\Delta\gamma_{xy}$ *X- and Y-axis perpendicularity error*
$\Delta\beta_{xz}$ *X and Z-axis perpendicularity error*
$\Delta\alpha_{yz}$ *Y and Z-axis perpendicularity error*
$\Delta\gamma_{xB}$ *B-axis parallelism error in the YZ plane*
$\Delta\alpha_{zB}$ *B-axis parallelism error in the XY plane*
$\Delta\gamma_{yA}$ *A-axis parallelism error in the XZ plane*
$\Delta\beta_{zA}$ *A-axis parallelism error in the XY plane*
Δy_{AB} *Offset errors between A- and B-axes along the Y-axis*
Δz_{AB} *Offset errors between A- and B-axes along the Z-axis*

1 Introduction

Due to high efficiency and capabilities of complex free form surface machining, the five-axis machining method is being used by machine tool users [28], increasingly. The design of a machine tool with satisfactory performance by cost-effective geometric accuracy configuration constitutes an intractable problem that machine tool manufacturers face. Machining accuracy is a key factor for the capability of five-axis machine tool evaluation, and it is taken into important consideration in an accurate design of machine tools [22]. Machining accuracy reliability reflects the capability of the required machining accuracy being reached for machine tools [1], and it is affected by factors having influence on machining accuracy, such as geometric, thermal-induced, cutting force-induced, and tool deflection errors [7]. Among these errors, both the geometric and the thermal errors are responsible for machine tool inaccuracy [21]. The cutting force-induced errors constitute another important error source, therefore proving to be a very critical problem in wide applications of both high-efficiency cutting and difficult-to-process materials [27]. As a conclusion, these three kinds of errors should be taken into consideration in accuracy design of machine tools. The manufacturing costs of machine tools depend on geometric errors of the main composing parts [9]; therefore, it has become necessary for optimum geometric errors of assembly component provision, for manufacturing cost minimization of the machine tool.

Two steps are included in machine tool accuracy design: accuracy prediction and accuracy allocation [17]. Accuracy prediction is the foundation of accuracy design, aiming in machine tool comprehensive error forecasting, explaining how machining accuracy is affected by various errors [5]. Nowadays, many modeling methods of machine tool comprehensive errors exist, such as the matrix translation method [16], the error matrix method [11], the rigid body kinematic method [26], the D-H method [19], the POE [5, 12, 13], and the multi-body system theory [23, 29, 30, 32, 38]. In the comprehensive error model, the geometric errors can be measured directly, whereas the thermal and cutting force-induced errors are obtained indirectly. Researches on thermal error focus mainly on two aspects. One aspect is the selection of temperature points such as the principal factor mutually uncorrelated and maximum sensitivity [35]. The second aspect is the thermal error modeling methods such as the fuzzy C means (FCM) clustering method [31], the ant-colony algorithm-based back-propagation neural network (ACOBPN), the synthetic grey correlation theory, the grey neural network [15, 37], and the RBF [6]. In recent years, the study of cutting force errors is mainly concentrated on modeling methods of cutting force errors, such as the particle swarm optimization (PSO)-SVM [14], the fuzzy neural network theory [4, 33], and the PSO-BP neural network [37]. However, the forehand mentioned references above display only a few kinds of error during machine tool error modeling. Therefore, one objective for execution of this research was the development of comprehensive error modeling of a machine tool with simultaneous consideration of geometric, thermal, and cutting force-induced errors.

Compared to accuracy prediction, accuracy allocation constitutes an optimization issue for the geometric errors in order for the machining accuracy reliability to be satisfied and the minimum cost of machine tools to be minimized [2]. Until recently, various cost-tolerance models were proposed for a proper functional relationship building between the manufacturing cost and geometric errors [9] to be estimated. Nowadays, both the reliability-based design optimization (RBDO) and the robust design optimization (RDO) are often combined as a tool to optimize the objective parameters, concerning the minimization of an objective function under probabilistic constraints evaluated by reliability and sensitivity analysis [8]. There are many important methods of reliability and sensitivity analysis such as differential analysis, response surface methodology, Monte Carlo analysis, and variance decomposition procedures [3], as methods having been widely used in the machine tool domain of interest. Besides, Dorndorf et al. proposed an error allocation approach for manufacturing and assembly tolerance allocation and determination of optimal levels for these errors [10]. Yu et al. proposed an accuracy allocation approach based on a geometric error propagation model and the response surface method, whereas following

improved the functions of a machine tool according to the reliability sensitivity analysis [36]. A scatter search method was used by Krishna et al. for allocation of geometric errors with a minimum total manufacturing cost preservation [18]. Jin et al. presented an accuracy design approach for automotive parts during an early design stage [20]. Cai et al. proposed an accuracy distribution method for machine tools by advanced first-order and second-moment (AFOSM) theory application [1] and formulated an accuracy retainability optimization approach based on the HOMST [2]. However, in the above studies, the influence of thermal and cutting force-induced errors to accuracy allocation of machine tools have not been considered. As a result, a continuous research effort of a reliability model for the development of a general accuracy allocation approach that simultaneously considers geometric, thermal, and cutting force-induced errors is sought.

This paper is divided into five sections: In Sect. 2, a comprehensive error model of a numerical control (NC) machine tool is established. In Sect. 3, two mathematical models, machine tool reliability prediction and error parameter optimization, are used, in order for a general accuracy allocation approach to be developed. In Sect. 4, a machining example in a five-axis machine tool was performed in order for the proposed approach to be verified. Following conclusions and suggestions for future studies are presented.

2 Comprehensive error modeling

In this paper, homogeneous transformation matrices (HTMs) are used for the establishment of a direct kinematic model that considers geometric, thermal, and cutting force-induced errors. A five-axis machine tool (XKH800), comprising three translational axes (*X*, *Y*, and *Z*) and two rotational axes (*A* and *B*), is presented in Fig.1a. The system structure coordination diagram of the machine, essentially being a serial-link mechanism, is shown in Fig. 1b.

2.1 Analysis of thermal and cutting force-induced errors

In the comprehensive error model, geometric, thermal, and cutting force-induced errors should be included. All these errors are necessary to be acquired in order for the comprehensive error model to be obtained. Geometric errors can be obtained by a direct measurement method from measurement tools such as the various laser interferometers. However, thermal and cutting force-induced errors cannot be obtained by the direct measurement method. As a result, a systemic method for thermal and cutting force-induced error modeling was applied, based on a generalized RBF [25].

Because each drive motor and bed body of this machine tool has been designed separately, a perfect structure for heat dissipation is being offered. The high-speed motorized spindle constitutes the most important part and the main source of heat. Consequently, the spindle has a larger impact than any other part during machining. Both thermal and cutting force-induced errors contribute to spindle errors in all axial X, Y, and Z directions, and both kinds of error can be considered [34]. Additionally, this machine tool has excellent rigidity; therefore, cutting force-induced errors are induced by the applied cutting force, so the analysis of the cutting force can be used for the cutting force-induced error prediction [34]. During thermal and cutting force-induced error modeling of the spindle, the temperature measurement point selection is clearly an important factor to the accuracy of the thermal and cutting force-induced error model [34, 35]. Besides, according to Metal Cutting Theory, factors such as workpiece materials, cutting tool materials, and cutting parameters (cutting velocity v, cutting depth a_p, and cutting feed f), which affect the cutting force, affect the cutting force-induced errors also [34]. However, too many input parameters will increase the model complexity, leading to training process difficulties. Following, the principal factor is used for the selection of temperature point optimization, revealing the relationship between each temperature point and thermal and force-induced errors [35]. Besides, both the cutting depth a_p and the cutting feed f, having a certain relevance to cutting force errors, were chosen for thermal and cutting force-induced error modeling [34].

2.2 Modeling of thermal and cutting force-induced errors

The functional structure of the proposed comprehensive error model, based on a generalized RBF as presented in Fig. 2, contains the n thermal and the force parameter inputs$X=[\mathrm{x}_1,\mathrm{x}_2,...,\mathrm{x}_n]^T$, the s hidden nodes, and the m outputs $Y=[y_1,y_2,\ldots,y_m]^T$. Inside the hidden layer, the $\mathbf{U}_j=[\mu_{1j},\mu_{2j},\ldots,\mu_{\mathrm{sj}}]^T$ is the weighing matrix of y_j, $\mu_{ij}$is the synaptic weight of the ith hidden node of y_j, and $\xi_i(i=1,2,\ldots,\mathrm{s})$ refers to the radial basis function of the ith hidden node that is defined as: $\xi_i(\|\boldsymbol{X}-\boldsymbol{G}_i\|)=\exp\left(-\frac{\|\boldsymbol{X}-\boldsymbol{G}_i\|^2}{2\lambda_i^2}\right)\quad(i=1,2,...,\mathrm{s})$ where $\boldsymbol{X}$ are the thermal and force parameter inputs, G_i refers to the data center, and λ_i denotes the expansion constant. Each radial basis function corresponds to one data center and one expansion constant.

The thermal and cutting force-induced error modeling and validation based on the generalized RBF can be divided into four steps:

1. The thermal and induced force error experiment should be conducted on a machine tool with adequate

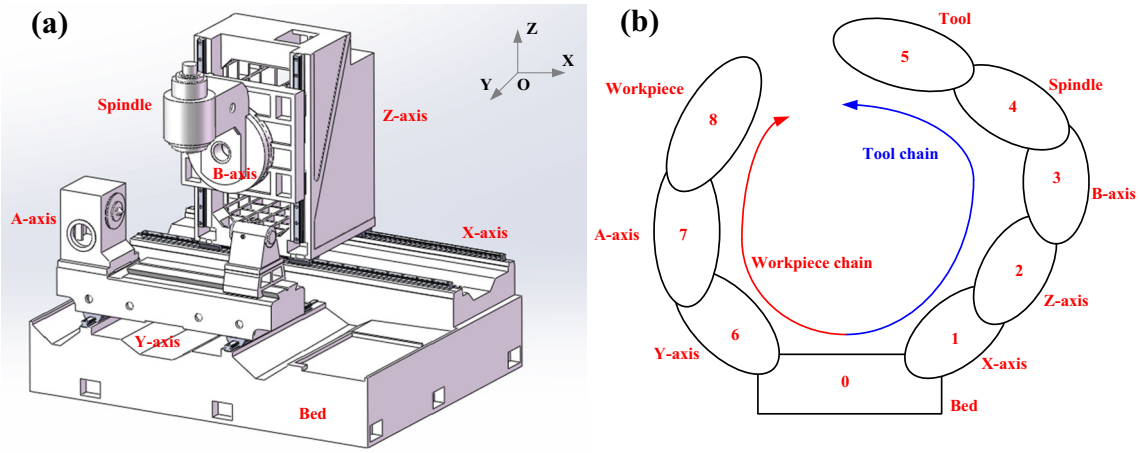

Fig. 1 Three-dimensional model of XKH800 and its system structure coordination diagram

temperature sensors and a laser interferometer that can be used for experimental data collection of both temperature and induced errors. The data are then divided into two groups. Both groups include r samples. The first group is used for sample training and the second for prediction ability verification of the model.

2. The number of data centers should be identified according to experimental results.
3. A K-means clustering algorithm is applied for the data centers and the expansion constants to be obtained. In order for the ideal data center to be determined, the Δx_z samples are randomly selected as the initial data centers $G_1(0), G_2(0), \ldots G_i(0), \ldots G_s(0)$ $(i=1,2,\ldots,s)$, from all samples of both thermal and force parameter input vectors X_q $(q=1,2,\ldots,r)$. Then, all samples are grouped in the Δx_B clustering domains $W_1(k), W_2(k), \ldots W_i(k), \ldots W_s(k)$ $(i=1,2,\ldots,s)$ by the European space distance of each sample left to the data centers $C_{qi}=\|X_q-\boldsymbol{G}_i\|$ $(q=1,2,\ldots,r;\ i=1,2,\ldots,s)$, when $\mathrm{Min}_p\, C_{qp}=C_{qi}$ $(p=1,2,\ldots,s)$. X_q belongs to G_i. Supposedly, k is the number of iterations, $W_i(k)$ is the *ith* clustering domain with the N_i sample number, and G_{def} is a precision object in this model previously set and then $G_i(k+1)=\frac{1}{N_i}\sum_{X\in W_i(k)} X$. When $\sum_{i=1}^{s}\|G_i(k+1)-G_i(k)\|<G_{\mathrm{def}}$, the ideal data centers $G_1(k+1), G_2(k+1), \ldots, G_i(k+1), \ldots, G_s(k+1)$ are acquired. Following the ideal data center determination, each expansion constant corresponding to each radial basis function can be obtained by the $\lambda_i=\alpha\times d_p$ equation, where $\alpha=0.2$ and $d_p=\min\|G_i-G_p\|$, substituted by the minimum European space distance of each data center.
4. Moreover, in calculation execution, μ_{ij} is obtained by the pseudo-inverse method. Considering that each output of this model can be expressed as a linear combination of the base function $\boldsymbol{y}_j=\sum_{i=1}^{s}\mu_{ij}\xi_i\|X-G_i\|$ $(j=1,2,\ldots,n)$

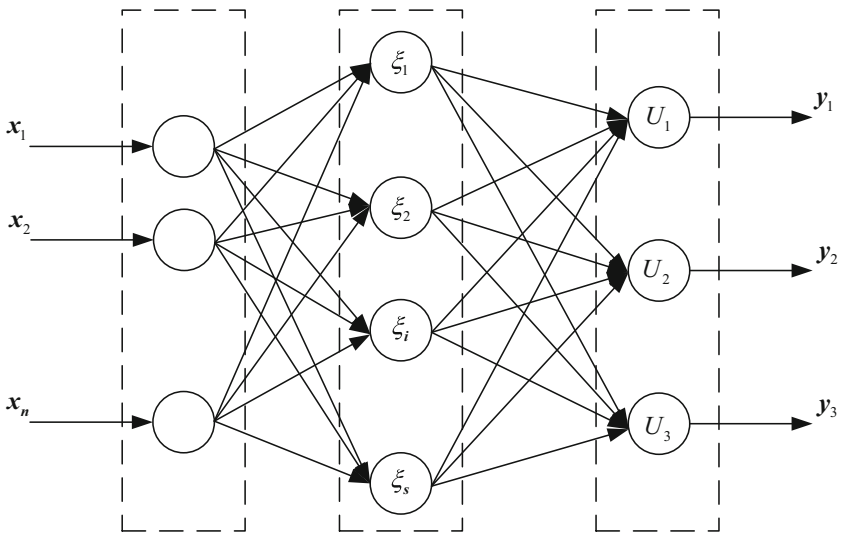

Fig. 2 The proposed comprehensive error model based on a generalized RBF

and the training samples(X_q, y_{qj}) (q = 1, 2, ... , r) of the *jth* output are inserted into the equation above, a system of linear equations regarding the unknown μ_{ij} can be obtained:

$$\begin{cases} y_{1j} = \sum_{i=1}^{s} \mu_{ij}\xi_i \|X_1 - G_i\| \\ y_{2j} = \sum_{i=1}^{s} \mu_{ij}\xi_i \|X_2 - G_i\| \quad (j = 1, 2, ..., n) \\ \vdots \\ y_{rj} = \sum_{i=1}^{s} \mu_{ij}\xi_i \|X_r - G_i\| \end{cases} \tag{1}$$

Accepting as an assumption that $\xi_{qi} = \xi_i \|X_q - G_i\|$. (q = 1, 2, .. , r; i = 1, 2, … , s), $y_j = [y_{1j}, y_{2j}, \ldots, y_{rj}]^T$, $\boldsymbol{U}_j = [\mu_{1j}, \mu_{2j}, \ldots, \mu_{sj}]^T$, and $\boldsymbol{\Psi}^{\wedge} = [\xi_{11}\ \xi_{12}\ \cdots \xi_{1s}\ \xi_{21}\ \xi_{22}\ \cdots \xi_{2s}\ \vdots\ \xi_{r1}\ \xi_{r2}\ \cdots \xi_{rs}]$, and Eq. (12) can be rewritten as $\boldsymbol{\Psi}^{\wedge}\mathbf{U}_j = y_j$. Thus, the weight matrix of the *jth* output can be acquired by the $\mathbf{U}_j = \boldsymbol{\Psi}^{\wedge +} y_j$ equation, where $\boldsymbol{\Psi}^{\wedge +} = \left(\boldsymbol{\Psi}^{\wedge T}\boldsymbol{\Psi}^{\wedge}\right)^{-1}\boldsymbol{\Psi}^{\wedge T}$ denotes the pseudo-inverse matrix of $\boldsymbol{\Psi}^{\wedge T}$.

So far, the ideal parameters of this model are obtained and can be consequently used for thermal and cutting force-induced error modeling. The rest of the group data can be used for verification of the developed model.

2.3 Comprehensive error modeling based on HTMs

Through forehand executed calculations, the geometric, thermal, and cutting force-induced errors were obtained. Therefore, a comprehensive error model of the machine tool foreseeing these errors was developed based on HTMs.

Regarding the spindle, the body kinematic error homogeneous transformation matrix can be written as

$$\Delta \boldsymbol{N}_{34S} = \begin{pmatrix} 1 & -\Delta\gamma_\varphi & \Delta\beta_\varphi & \Delta x_\varphi \\ \Delta\gamma_\varphi & 1 & -\Delta\alpha_\varphi & \Delta y_\varphi \\ -\Delta\beta_\varphi & \Delta\alpha_\varphi & 1 & \Delta z_\varphi \\ 0 & 0 & 0 & 1 \end{pmatrix} \tag{2}$$

Equation (2) contains three parts: geometric, thermal, and cutting force-induced errors. Therefore, it can be rewritten as

$$\Delta \boldsymbol{N}_{34\boldsymbol{S}} = \begin{pmatrix} 1 & -\left(\Delta\gamma_\varphi^g + \Delta\gamma_\varphi^t + \Delta\gamma_\varphi^f\right) & \Delta\beta_\varphi^g + \Delta\beta_\varphi^t + \Delta\beta_\varphi^f & \Delta x_\varphi^g + \Delta x_\varphi^t + \Delta x_\varphi^f \\ \Delta\gamma_\varphi^g + \Delta\gamma_\varphi^t + \Delta\gamma_\varphi^f & 1 & -\left(\Delta\alpha_\varphi^g + \Delta\alpha_\varphi^t + \Delta\alpha_\varphi^f\right) & \Delta y_\varphi^g + \Delta y_\varphi^t + \Delta y_\varphi^f \\ -\left(\Delta\beta_\varphi^g + \Delta\beta_\varphi^t + \Delta\beta_\varphi^f\right) & \Delta\alpha_\varphi^g + \Delta\alpha_\varphi^t + \Delta\alpha_\varphi^f & 1 & \Delta z_\varphi^g + \Delta z_\varphi^t + \Delta z_\varphi^f \\ 0 & 0 & 0 & 1 \end{pmatrix} \tag{3}$$

where *g*, *t*, and *f* refer to the geometric, thermal, and cutting force-induced errors, respectively.

Hypothetically, the coordinates of tool forming pointing the tool coordinate system are

$$P_t = \begin{bmatrix} P_{tx} & P_{ty} & P_{tz} & 1 \end{bmatrix}^T \tag{4}$$

The coordinates of the workpiece forming point in the workpiece coordinate system are

$$P_w = \begin{bmatrix} P_{wx} & P_{wy} & P_{wz} & 1 \end{bmatrix}^T \tag{5}$$

When the machine tool is operating in an ideal model, subsequently the machine tool has no errors and both the tool forming point and the workpiece forming point will overlap. Therefore, the following equation can be obtained:

$$\boldsymbol{N}_{\text{Tool}}\boldsymbol{P}_t = \boldsymbol{N}_{\text{Workpiece}}\boldsymbol{P}_{\text{wideal}} \tag{6}$$

where $\boldsymbol{N}_{\text{Tool}}$ is the homogenous transformation matrix of the tool branch and $\boldsymbol{N}_{\text{Workpiece}}$ is the homogenous transformation matrix of the workpiece branch. Then, the result will be

$$\begin{aligned} &\boldsymbol{N}_{0,1}^P \boldsymbol{N}_{0,1}^S \boldsymbol{N}_{1,2}^P \boldsymbol{N}_{1,2}^S \boldsymbol{N}_{2,3}^P \boldsymbol{N}_{2,3}^S \boldsymbol{N}_{3,4}^P \boldsymbol{N}_{3,4}^S \boldsymbol{N}_{4,5}^P \boldsymbol{N}_{4,5}^S \boldsymbol{P}_t \\ &= \boldsymbol{N}_{0,6}^P \boldsymbol{N}_{0,6}^S \boldsymbol{N}_{6,7}^P \boldsymbol{N}_{6,7}^S \boldsymbol{N}_{7,8}^P \boldsymbol{N}_{7,8}^S \boldsymbol{P}_{\text{wideal}} \end{aligned} \tag{7}$$

In Eq. (7), *P* and *S* are static and motion transformations, respectively, where $\boldsymbol{N}_{J\text{-}1,J}^P$ refers to the ideal static homogenous transformation matrix of the adjacent body and $\boldsymbol{N}_{J\text{-}1,J}^S$ refers to the ideal motion homogenous transformation matrix of the adjacent body, as presented in Table 1. From Eq. (7) it can be derived that the coordinates of the ideal tool forming point in the workpiece coordinate system can be obtained as follows:

$$\begin{aligned} \boldsymbol{P}_{\text{wideal}} = &\left(\boldsymbol{N}_{0,6}^P \boldsymbol{N}_{0,6}^S \boldsymbol{N}_{6,7}^P \boldsymbol{N}_{6,7}^S \boldsymbol{N}_{7,8}^P \boldsymbol{N}_{7,8}^S\right)^{-1} \\ &\boldsymbol{N}_{0,1}^P \boldsymbol{N}_{0,1}^S \boldsymbol{N}_{1,2}^P \boldsymbol{N}_{1,2}^S \boldsymbol{N}_{2,3}^P \boldsymbol{N}_{2,3}^S \boldsymbol{N}_{3,4}^P \boldsymbol{N}_{3,4}^S \boldsymbol{N}_{4,5}^P \boldsymbol{N}_{4,5}^S \boldsymbol{P}_t \end{aligned} \tag{8}$$

Table 1 The ideal and the error homogenous transformation matrices of the machine tool

Sdjacent body	Body ideal static, motion HTMs ($\boldsymbol{N}^{P}_{J\text{-}1,J}$, $\boldsymbol{N}^{S}_{J\text{-}1,J}$)	Body static, motion error HTMs (${}^{e}\boldsymbol{N}^{P}_{J\text{-}1,J}$, ${}^{e}\boldsymbol{N}^{S}_{J\text{-}1,J}$)
0–1 X-axis	$\boldsymbol{N}^{P}_{0,1}=\boldsymbol{I}_{4\times4}$	${}^{e}\boldsymbol{N}^{P}_{0,1}=\boldsymbol{I}_{4\times4}$
	$\boldsymbol{N}^{S}_{0,1}=\begin{pmatrix}1&0&0&x\\0&1&0&0\\0&0&1&0\\0&0&0&1\end{pmatrix}$	${}^{e}\boldsymbol{N}^{S}_{0,1}=\begin{pmatrix}1&-\Delta\gamma_x&\Delta\beta_x&\Delta x_x\\\Delta\gamma_x&1&-\Delta\alpha_x&\Delta y_x\\-\Delta\beta_x&\Delta\alpha_x&1&\Delta z_x\\0&0&0&1\end{pmatrix}$
1–2 Z-axis	$\boldsymbol{N}^{P}_{1,2}=\boldsymbol{I}_{4\times4}$	${}^{e}\boldsymbol{N}^{P}_{1,2}=\begin{pmatrix}1&0&\Delta\beta_{xz}&0\\0&1&-\Delta\alpha_{yz}&0\\-\Delta\beta_{xz}&\Delta\alpha_{yz}&1&0\\0&0&0&1\end{pmatrix}$
	$\boldsymbol{N}^{S}_{1,2}=\begin{pmatrix}1&0&0&0\\0&1&0&0\\0&0&1&z\\0&0&0&1\end{pmatrix}$	${}^{e}\boldsymbol{N}^{S}_{1,2}=\begin{pmatrix}1&-\Delta\gamma_z&\Delta\beta_z&\Delta x_z\\\Delta\gamma_z&1&-\Delta\alpha_z&\Delta y_z\\-\Delta\beta_z&\Delta\alpha_z&1&\Delta z_z\\0&0&0&1\end{pmatrix}$
2–3 B-axis	$\boldsymbol{N}^{P}_{2,3}=\boldsymbol{I}_{4\times4}$	${}^{e}\boldsymbol{N}^{p}_{2,3}=\begin{pmatrix}1&-\Delta\gamma_{xB}&0&0\\\Delta\gamma_{xB}&1&-\Delta\alpha_{zB}&0\\0&\Delta\alpha_{zB}&1&\Delta z_{AB}\\0&0&0&1\end{pmatrix}$
	$\boldsymbol{N}^{S}_{2,3}=\begin{pmatrix}\cos B&0&\sin B&0\\0&1&0&0\\-\sin B&0&\cos B&0\\0&0&0&1\end{pmatrix}$	${}^{e}\boldsymbol{N}^{S}_{2,3}=\begin{pmatrix}1&-\Delta\gamma_B&\Delta\beta_B&\Delta x_B\\\Delta\gamma_B&1&-\Delta\alpha_B&\Delta y_B\\-\Delta\beta_B&\Delta\alpha_B&1&\Delta z_B\\0&0&0&1\end{pmatrix}$
3–4 Spindle	$\boldsymbol{N}^{P}_{3,4}=\boldsymbol{I}_{4\times4}$	${}^{e}\boldsymbol{N}^{P}_{3,4}=\boldsymbol{I}_{4\times4}$
	$\boldsymbol{N}^{S}_{3,4}=\begin{pmatrix}\cos\varphi&\sin\varphi&0&0\\-\sin\varphi&\cos\varphi&0&0\\0&0&1&0\\0&0&0&1\end{pmatrix}$	${}^{e}\boldsymbol{N}^{S}_{3,4}=\begin{pmatrix}1&-\Delta\gamma_\varphi&\Delta\beta_\varphi&\Delta x_\varphi\\\Delta\gamma_\varphi&1&-\Delta\alpha_\varphi&\Delta y_\varphi\\-\Delta\beta_\varphi&\Delta\alpha_\varphi&1&\Delta z_\varphi\\0&0&0&1\end{pmatrix}$
4–5 Tool	$\boldsymbol{N}^{P}_{4,5}=\begin{pmatrix}1&0&0&x_{td}\\0&1&0&L+y_{td}\\0&0&1&z_{td}\\0&0&0&1\end{pmatrix}$	${}^{e}\boldsymbol{N}^{P}_{4,5}=\begin{pmatrix}1&-\Delta\gamma_{td}&\Delta\beta_{td}&\Delta x_{td}\\\Delta\gamma_{td}&1&-\Delta\alpha_{td}&\Delta y_{td}\\-\Delta\beta_{td}&\Delta\alpha_{td}&1&\Delta z_{td}\\0&0&0&1\end{pmatrix}$
	$\boldsymbol{N}^{S}_{4,5}=\boldsymbol{I}_{4\times4}$	${}^{e}\boldsymbol{N}^{S}_{4,5}=\boldsymbol{I}_{4\times4}$
0–6 Y-axis	$\boldsymbol{N}^{P}_{0,6}=\boldsymbol{I}_{4\times4}$	${}^{e}\boldsymbol{N}^{P}_{0,6}=\begin{pmatrix}1&-\Delta\gamma_{xy}&0&0\\\Delta\gamma_{xy}&1&0&0\\0&0&1&0\\0&0&0&1\end{pmatrix}$
	$\boldsymbol{N}^{S}_{0,6}=\begin{pmatrix}1&0&0&0\\0&1&0&y\\0&0&1&0\\0&0&0&1\end{pmatrix}$	${}^{e}\boldsymbol{N}^{S}_{0,6}=\begin{pmatrix}1&-\Delta\gamma_y&\Delta\beta_y&\Delta x_y\\\Delta\gamma_y&1&-\Delta\alpha_y&\Delta y_y\\-\Delta\beta_y&\Delta\alpha_y&1&\Delta z_y\\0&0&0&1\end{pmatrix}$
6–7 A-axis	$\boldsymbol{N}^{P}_{6,7}=\boldsymbol{I}_{4\times4}$	${}^{e}\boldsymbol{N}^{p}_{6,7}=\begin{pmatrix}1&-\Delta\gamma_{yA}&\Delta\beta_{zA}&0\\\Delta\gamma_{yA}&1&0&\Delta y_{AB}\\-\Delta\beta_{zA}&0&1&0\\0&0&0&1\end{pmatrix}$
	$\boldsymbol{N}^{S}_{6,7}=\begin{bmatrix}1&0&0&0\\0&\cos A&-\sin A&0\\0&\sin A&\cos A&0\\0&0&0&1\end{bmatrix}$	

Table 1 (continued)

Sdjacent body	Body ideal static, motion HTMs ($\boldsymbol{N}^{P}_{J\text{-}1,J}$, $\boldsymbol{N}^{S}_{J\text{-}1,J}$)	Body static, motion error HTMs (${}^{e}\boldsymbol{N}^{P}_{J\text{-}1,J}$, ${}^{e}\boldsymbol{N}^{S}_{J\text{-}1,J}$)
		${}^{e}\boldsymbol{N}^{S}_{6,7} = \begin{bmatrix} 1 & -\Delta\gamma_a & \Delta\beta_a & \Delta x_a \\ \Delta\gamma_a & 1 & -\Delta\alpha_a & \Delta y_a \\ -\Delta\beta_a & \Delta\alpha_a & 1 & \Delta z_a \\ 0 & 0 & 0 & 1 \end{bmatrix}$
7–8 Workpiece	$\boldsymbol{N}^{P}_{7,8} = \begin{pmatrix} 1 & 0 & 0 & x_{wd} \\ 0 & 1 & 0 & y_{wd} \\ 0 & 0 & 1 & z_{wd} \\ 0 & 0 & 0 & 1 \end{pmatrix}$	${}^{e}\boldsymbol{N}^{P}_{7,8} = \begin{pmatrix} 1 & -\Delta\gamma_{wd} & \Delta\beta_{wd} & \Delta x_{wd} \\ \Delta\gamma_{wd} & 1 & -\Delta\alpha_{wd} & \Delta y_{wd} \\ -\Delta\beta_{wd} & \Delta\alpha_{wd} & 1 & \Delta z_{wd} \\ 0 & 0 & 0 & 1 \end{pmatrix}$
	$\boldsymbol{N}^{S}_{7,8}=\boldsymbol{I}_{4\times4}$	${}^{e}\boldsymbol{N}^{S}_{7,8}=\boldsymbol{I}_{4\times4}$

However, when errors enter the system, both static and motion transformations become perturbed. As a result, the coordinates of the actual tool forming point in the coordinate system of the workpiece can be expressed as

$$\boldsymbol{P}_{w\text{actual}} = \left({}^{\mathrm{E}}\boldsymbol{N}_{\mathrm{Workpiece}}\right)^{-1}{}^{\mathrm{E}}\boldsymbol{N}_{\mathrm{Tool}}\boldsymbol{P}_{t} \tag{9}$$

In Eq. (9), the error homogenous transformation matrix of the workpiece branch ${}^{E}\boldsymbol{N}_{\mathrm{Workpiece}}$ and the error homogenous transformation matrix of the tool branch ${}^{E}\boldsymbol{N}_{\mathrm{Tool}}$ can be described as

$$\begin{aligned} {}^{\mathrm{E}}\boldsymbol{N}_{\mathrm{Workpiece}} &= \boldsymbol{N}^{P}_{0,6}\cdot{}^{e}\boldsymbol{N}^{P}_{0,6}\cdot\boldsymbol{N}^{S}_{0,6}\cdot{}^{e}\boldsymbol{N}^{S}_{0,6}\cdot\boldsymbol{N}^{P}_{6,7}\cdot{}^{e}\boldsymbol{N}^{P}_{6,7}\cdot\boldsymbol{N}^{S}_{6,7}\cdot{}^{e}\boldsymbol{N}^{S}_{6,7} \\ &\quad\cdot\boldsymbol{N}^{p}_{7,8}\cdot{}^{e}\boldsymbol{N}^{p}_{7,8}\cdot\boldsymbol{N}^{S}_{7,8}\cdot{}^{e}\boldsymbol{N}^{S}_{7,8} \\ {}^{\mathrm{E}}\boldsymbol{N}_{\mathrm{Tool}} &= \boldsymbol{N}^{p}_{0,1}\cdot{}^{e}\boldsymbol{N}^{p}_{0,1}\cdot\boldsymbol{N}^{s}_{0,1}\cdot{}^{e}\boldsymbol{N}^{s}_{0,1}\cdot\boldsymbol{N}^{p}_{1,2}\cdot{}^{e}\boldsymbol{N}^{p}_{1,2}\cdot\boldsymbol{N}^{s}_{1,2}\cdot{}^{e}\boldsymbol{N}^{s}_{1,2}\cdot \\ &\quad\boldsymbol{N}^{p}_{2,3}\cdot{}^{e}\boldsymbol{N}^{p}_{2,3}\cdot\boldsymbol{N}^{s}_{2,3}\cdot{}^{e}\boldsymbol{N}^{s}_{2,3}\cdot \\ &\quad\boldsymbol{N}^{p}_{3,4}\cdot{}^{e}\boldsymbol{N}^{p}_{3,4}\cdot\boldsymbol{N}^{s}_{3,4}\cdot{}^{e}\boldsymbol{N}^{s}_{3,4}\cdot\boldsymbol{N}^{p}_{4,5}\cdot{}^{e}\boldsymbol{N}^{p}_{4,5}\cdot\boldsymbol{N}^{s}_{4,5}\cdot{}^{e}\boldsymbol{N}^{s}_{4,5} \end{aligned} \tag{10}$$

In Eq. (10), ${}^{e}\boldsymbol{N}^{P}_{J\text{-}1,J}$ and ${}^{e}\boldsymbol{N}^{S}_{J\text{-}1,J}$ refer to the static error homogenous transformation matrix and the motion error

Table 2 Initial values of geometric parameter errors of the five-axis NC machine tool

Number *i*	1	2	3	4	5	6	7	8
Parameter	Δx_x	Δy_x	Δz_x	Δa_x	$\Delta\beta_x$	$\Delta\gamma_x$	Δx_y	Δy_y
Value	0.0062 mm	0.0062 mm	0.0062 mm	$\left(\frac{0.0035}{1000}\right)^{\circ}$	$\left(\frac{0.0035}{1000}\right)^{\circ}$	$\left(\frac{0.0035}{1000}\right)^{\circ}$	0.0064 mm	0.0064 mm
Number *i*	9	10	11	12	13	14	15	16
Parameter	Δz_y	Δa_y	$\Delta\beta_y$	$\Delta\gamma_y$	Δx_y	Δy_z	Δz_z	Δa_z
Value	0.0064 mm	$\left(\frac{0.0025}{1000}\right)^{\circ}$	$\left(\frac{0.0025}{1000}\right)^{\circ}$	$\left(\frac{0.0025}{1000}\right)^{\circ}$	0.0064 mm	0.0064 mm	0.0064 mm	$\left(\frac{0.0026}{1000}\right)^{\circ}$
Number *i*	17	18	19	20	21	22	23	24
Parameter	Δx_A	$\Delta\gamma_z$	Δx_φ	Δy_φ	Δz_φ	$\Delta\alpha_\varphi$	$\Delta\beta_\varphi$	$\Delta\gamma_\varphi$
Value	$\left(\frac{0.0026}{1000}\right)^{\circ}$	$\left(\frac{0.0026}{1000}\right)^{\circ}$	0.0053 mm	0.0053 mm	0.0053 mm	$\left(\frac{0.0058}{1000}\right)^{\circ}$	$\left(\frac{0.0058}{1000}\right)^{\circ}$	$\left(\frac{0.0058}{1000}\right)^{\circ}$
Number *i*	25	26	27	28	29	30	31	32
Parameter	Δx_A	Δy_A	Δz_A	Δa_A	$\Delta\beta_A$	$\Delta\gamma_A$	Δx_B	Δy_B
Value	0.0055 mm	0.0055 mm	0.0055 mm	Δy_φ	Δz_φ	$\Delta\alpha_\varphi$	0.0064 mm	0.0064 mm
Number *i*	33	34	35	36	37	38	39	40
Parameter	Δz_B	Δa_B	$\Delta\beta_B$	$\Delta\gamma_B$	$\Delta\gamma_{xy}$	$\Delta\beta_{xz}$	Δa_{yz}	$\Delta\gamma_{yA}$
Value	0.0064 mm	$\left(\frac{0.0047}{1000}\right)^{\circ}$	$\left(\frac{0.0047}{1000}\right)^{\circ}$	$\left(\frac{0.0047}{1000}\right)^{\circ}$	$\left(\frac{0.0034}{500}\right)^{\circ}$	$\left(\frac{0.0034}{500}\right)^{\circ}$	$\left(\frac{0.0034}{500}\right)^{\circ}$	$\left(\frac{0.009}{300}\right)^{\circ}$
Number *i*	41	42	43	44	45			
Parameter	$\Delta\beta_{zA}$	$\Delta\gamma_{xB}$	$\Delta\alpha_{zB}$	Δy_{AB}	Δz_{AB}			
Value	$\left(\frac{0.009}{300}\right)^{\circ}$	$\left(\frac{0.009}{300}\right)^{\circ}$	$\left(\frac{0.009}{300}\right)^{\circ}$	0.0064 mm	0.0064 mm			

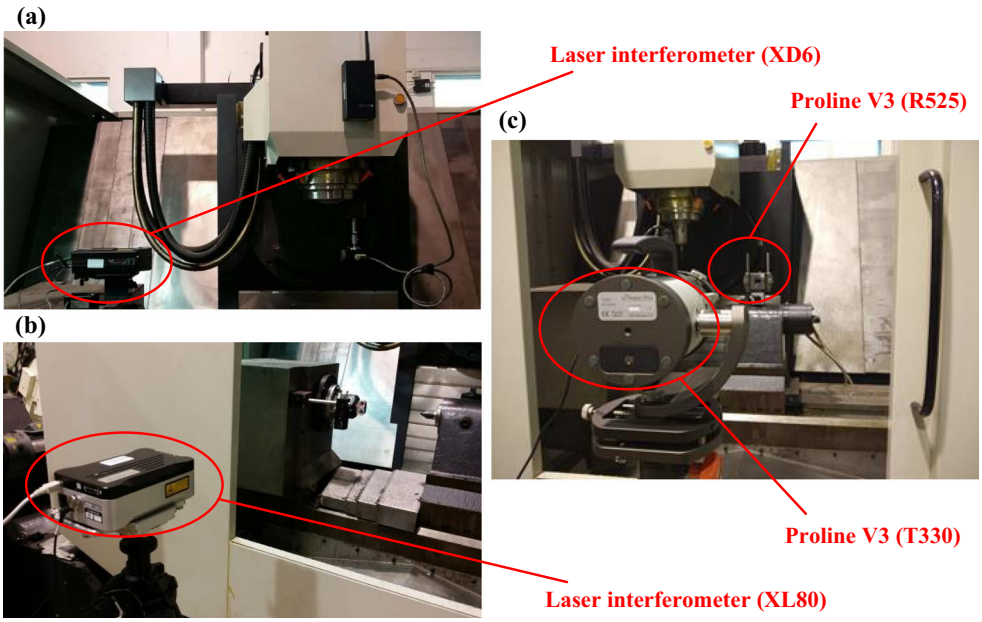

Fig. 3 Measurement methods of geometric errors: **a** Prismatic joint error measurement. **b** Rotary joint error measurement. **c** Squareness and offset error measurement

homogenous transformation matrix of the adjacent body, respectively, as presented in Table 1. The definitions of all the errors in Table 1 are presented in a nomenclature, which have been justified in usage according to [21]. Both thermal and cutting force-induced errors have been justified in usage according to [34].

The comprehensive error model of the five-axis machine tool caused by the value difference between actual and ideal forming points can be obtained by

$$\boldsymbol{E} = {}^{\mathrm{E}}\boldsymbol{N}_{\mathrm{Workpiece}}\boldsymbol{P}_{\mathrm{wideal}} - {}^{\mathrm{E}}\boldsymbol{N}_{\mathrm{Tool}}\boldsymbol{P}_{t} \tag{11}$$

where the $\boldsymbol{E}$ represents the comprehensive error of this machine tool, containing in turn the $\boldsymbol{E}_{\mathrm{x}}$, $\boldsymbol{E}_{\mathrm{y}}$, and$\boldsymbol{E}_{\mathrm{z}}$ parts. Following, Eq. (11) can be expressed as

$$\boldsymbol{E} = \left[\boldsymbol{E}_{\mathrm{x}}, \boldsymbol{E}_{y}, \boldsymbol{E}_{z}, 0\right]^{T} \tag{12}$$

3 Reliability and sensitivity analysis based on importance sampling method

3.1 Reliability and sensitivity analysis during single failure mode

The reliability of the structure reflects the ability of its specified functions under the stated conditions to be performed, for a specific period. It is often expressed through failure possibility. In order for this ability of machine tools to be reflected, the possibility of the specified machining accuracy having been met was taken as the basis of evaluating machining accuracy performance [7].

According to the logical relationship of the failure modes, a machine tool has multiple failure modes as a serial system. Therefore, the importance sampling method, used for the reliability and sensitivity analysis with

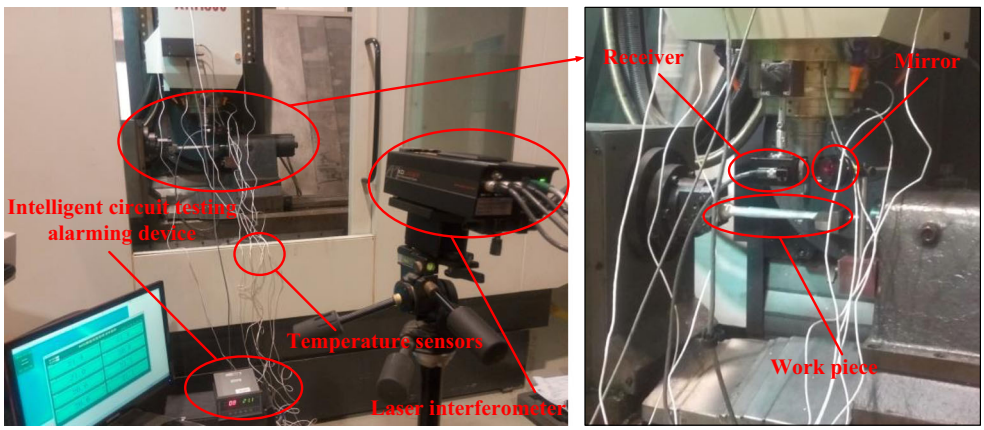

Fig. 4 The thermal and force-induced error experiment

Table 3 The machining parameters of the thermal and cutting force-induced error prediction test

Speed of the spindle (r/min)	Cutting depth (mm)	Cutting feed (mm/min)
2000	0.3, 0.4, 0.5, 0.7, 0.8, 0.9, 1, 2, 3, 5, 5.5, 6	20, 30, 40, 50

multiple failure modes, was introduced. The solution procedure follows the approach developed roughly ([24]), but differs in the used formulation.

The failure possibility of the single failure mode, based on the importance sampling method, is

$$P = \int\cdots\int_{R^n} I_F(x) f_X(x) dx = \int\cdots\int_{R^n} I_F(x) \frac{f_X(x)}{h_X(x)} h_X(x) dx = E\left[I_F(x)\frac{f_X(x)}{h_X(x)}\right] \tag{13}$$

where R^n, $f_X(x)$, and $h_X(x)$ refer to a variable space with n dimensions, the joint possibility density function, and the importance sampling density function, respectively.

According to $h_X(x)$, a sample space of size N and the sample points $x_i (i = 1, 2, \ldots, N)$ are selected. Eq. (13) can be rewritten as

$$\hat{P} = \frac{1}{N}\sum_{i=1}^{N} I_F(x_i)\frac{f_X(x_i)}{h_X(x_i)} \tag{14}$$

The mathematical expectation and variance of $P^{\wedge}$ can now be specified as follows:

$$E\left(\hat{P}\right) = E\left[\frac{1}{N}\sum_{i=1}^{N} I_F(x_i)\frac{f_X(x_i)}{h_X(x_i)}\right] = E\left[I_F(x_i)\frac{f_X(x_i)}{h_X(x_i)}\right] = P \tag{15}$$

$$\begin{aligned} Var\left(\hat{P}\right) &= Var\left[\frac{1}{N}\sum_{i=1}^{N} I_F(x_i)\frac{f_X(x_i)}{h_X(x_i)}\right] = \frac{1}{N^2}\sum_{i=1}^{N} Var\left[I_F(x_i)\frac{f_X(x_i)}{h_X(x_i)}\right] \\ &= \frac{1}{N} Var\left[I_F(x_i)\frac{f_X(x_i)}{h_X(x_i)}\right] = \frac{1}{N} Var\left[I_F(x)\frac{f_X(x)}{h_X(x)}\right] \\ &\approx \frac{1}{N-1}\left\{\frac{1}{N}\sum_{i=1}^{N}\left[I_F(x_i)\frac{f_X(x_i)}{h_X(x_i)}\right]^2 - \left[\frac{1}{N}\sum_{i=1}^{N} I_F(x_i)\frac{f_X(x_i)}{h_X(x_i)}\right]^2\right\} \\ &\approx \frac{1}{N-1}\left[\frac{1}{N}\sum_{i=1}^{N} I_F(x_i)\frac{f_X^2(x_i)}{h_X^2(x_i)} - P^2\right] \end{aligned} \tag{16}$$

Compared to machining accuracy reliability as a specification measurement for the ability of the machine tool to overcome a certain function, the machining accuracy sensitivity reflects the influence of the basic geometric error to the possibility of failure that can be used for improving and optimizing the geometric errors of the machine tool [7]. From the following equations, the reliability sensitivity $\frac{\partial P}{\partial \theta_{x_i}^{(k)}}$ and the corresponding estimated value $\frac{\partial \boldsymbol{P}}{\partial \theta_{\boldsymbol{x_i}}^{(\boldsymbol{k})}}$ can be expressed as

$$\begin{aligned} \frac{\partial P}{\partial \theta_{x_i}^{(k)}} &= \int\cdots\int_{R^n} I_F(x)\frac{\partial f_X(x)}{\partial \theta_{x_i}^{(k)}} dx \\ &= \int\cdots\int_{R^n} \frac{\partial f_X(x)}{\partial \theta_{x_i}^{(k)}}\frac{I_F(x)}{h_X(x)} h_X(x) dx = E\left[\frac{I_F(x)}{h_X(x)}\frac{\partial f_X(x)}{\partial \theta_{x_i}^{(k)}}\right] \end{aligned} \tag{17}$$

$$\frac{\hat{\partial P}}{\partial \theta_{x_i}^{(k)}} = \frac{1}{N}\sum_{j=1}^{N}\frac{I_F(x_j)}{h_X(x_j)}\frac{\partial f_X(x)}{\partial \theta_{x_i}^{(k)}}\Big|_{x=x_j} \tag{18}$$

where $x = (x_1, x_2, \ldots, x_n)^T$ are uncorrelated parameters drawn from the random distribution $x_i \sim N\left(\mu_{x_i}, \sigma_{x_i}^2\right)$; the estimated value $\frac{\partial P}{\partial \theta_{x_i}^{(k)}}^{\wedge}$ can be simplified into the following two equations:

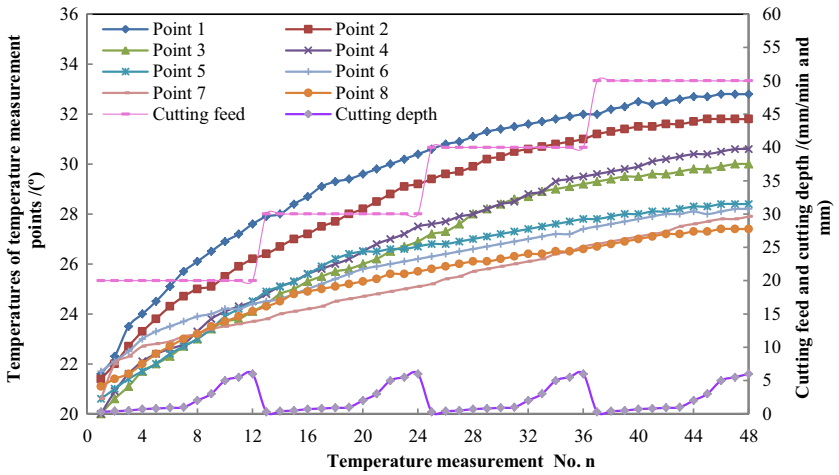

Fig. 5 Data of eight temperature points and two cutting force-induced error collected parameters

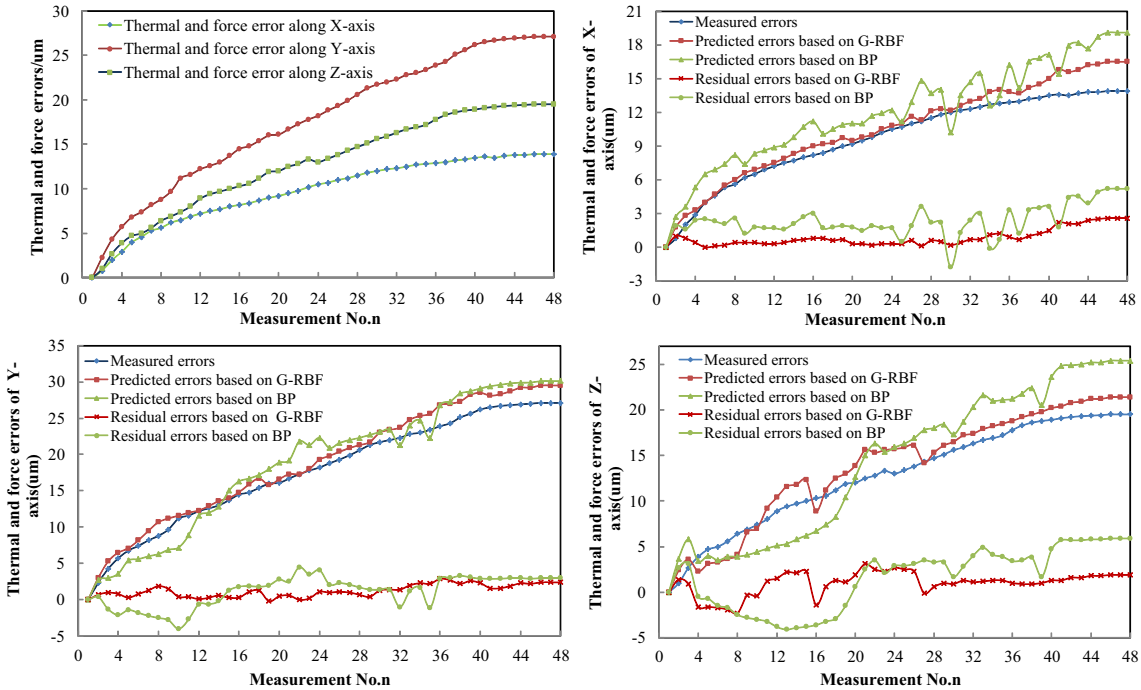

Fig. 6 Results of the thermal and force-induced errors experiment

$$\frac{\partial \hat{P}}{\partial \mu_{x_i}} = \frac{1}{N}\sum_{j=1}^{N} \frac{I_F(x_j) f_X(x_j)(x_{ji} - \mu_{x_i})}{h_X(x_j)\sigma_{x_i}^2} \tag{19}$$

$$\frac{\partial \hat{P}}{\partial \sigma_{x_i}} = \frac{1}{N}\sum_{j=1}^{N} \frac{I_F(x_j) f_X(x_j)}{\sigma_{x_i} h_X(x_j)} \left[\frac{(x_{ji} - \mu_{x_i})^2}{\sigma_{x_i}^2} - 1 \right] \tag{20}$$

3.2 Reliability and sensitivity analysis with multiple failure modes

Hypothetically, "m" failure modes exist and each performance function of these modes is described as $g^{(k)}(x) = 0 (k = 1, 2, \ldots, m)$ with the use of the reliability index β_k. Considering that different failure modes have different contributions to the systemic failure possibility, a comprehensive importance sampling density function is necessary to be constructed through the weight of each failure mode, according to individual contributions to the failure possibility. The expression for the failure possibility of each failure mode is the approximate $\Phi(-\beta_k)$, whereas the weight of each failure mode can therefore be expressed as

$$\alpha_k = \frac{\Phi(-\beta_k)}{\sum_{j=1}^{m} \Phi(-\beta_k)}, k = 1, 2, \ldots, m \tag{21}$$

A comprehensive importance sampling density function by use of the weight of each failure mode can be obtained:

$$h_X(x) = \sum_{k=1}^{m} \alpha_k h_X^{(k)}(x) = \sum_{k=1}^{m} \frac{\Phi(-\beta_k)}{\sum_{j=1}^{m} \Phi(-\beta_k)} h_X^{(k)}(x) \tag{22}$$

where $h_X^{(k)}(x)$ is the importance sampling density function of each failure. It is often constructed by a corresponding center placement on the design point (the most probable failure point), a center that cannot be obtained accurately. In order for the efficiency and accuracy of systemic failure possibility ensuring to be improved, the kernel importance sampling density function is introduced and consequently used for reliability and sensitivity analysis. Regarding the lack of space, a description of the complete

Table 4 Performance comparison of two network models (unit: μm)

	Network type	Maximum absolute deviation	Mean square error
X-axis	Residual errors (BP)	5.2	1.415264
	Residual errors (G-RBF)	2.6	0.767672
Y-axis	Residual errors (BP)	4.5	2.129253
	Residual errors (G-RBF)	2.9	0.856721
Z-axis	Residual errors (BP)	5.9	3.359283
	Residual errors (G-RBF)	3.1	1.287411

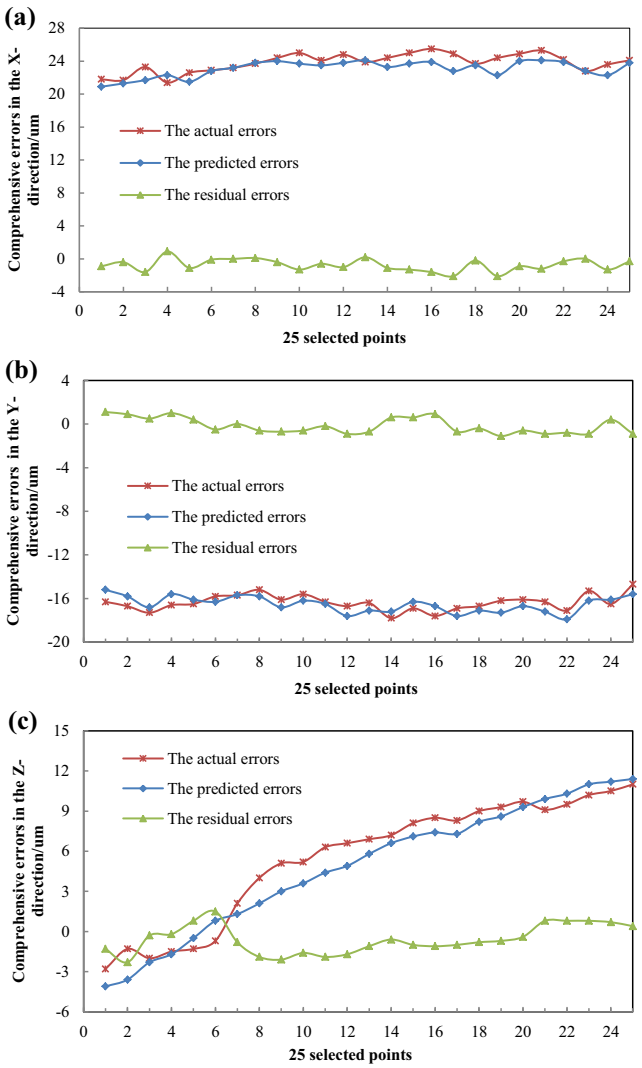

Fig. 7 Comprehensive errors: **a** the errors in the X-axis direction; **b** the errors in the Y-axis direction; **c** the errors in the Z-axis direction

theoretical analysis is avoided and only some important results are given, as follows:

$$h_X^{(k)}(x) = \frac{1}{M^{(k)}} \sum_{i=1}^{M^{(k)}} \frac{1}{\omega^{(k)}} \left[\frac{1}{\sqrt{2\pi}} \exp \frac{1}{2} \left(\frac{x^{(k)} - y_i^{(k)}}{\omega^{(k)}} \right)^2 \right] \tag{23}$$

where $M^{(k)}$ refers to the kernel sample size, $\omega^{(k)}$ is the bandwidth that can be obtained from the integral square-error method, and $y_i^{(k)}$ denotes the sample value of the Monte Carlo method.

As a result, the systemic failure possibility P_t and the deriving estimated value can be obtained:

$$P = \int \cdots \int_{R^n} I_F(x) \frac{f_X(x)}{h_X(x)} \sum_{k=1}^{m} \alpha_k h_X^{(k)}(x) dx = \sum_{k=1}^{m} E\left[I_F(x) \frac{f_X(x)}{h_X(x)} \alpha_k \right]_{h_X^{(k)}(x)} \tag{24}$$

$$\hat{P} = \sum_{k=1}^{m} \frac{1}{N_k} \sum_{j=1}^{N_k} I_F\left(x_j^{(k)}\right) \frac{f_X\left(x_j^{(k)}\right)}{h_X\left(x_j^{(k)}\right)} \alpha_k \tag{25}$$

Subsequently, the sensitivity and derived estimated values according to Eq. (24) are given:

$$\frac{\partial P}{\partial \theta_{x_i}^{(k)}} = \int \cdots \int_{R^n} \frac{\partial f_X(x)}{\partial \theta_{x_i}^{(k)}} \frac{I_F(x)}{h_X(x)} \sum_{k=1}^{m} \alpha_k h_X^{(k)}(x) dx = \sum_{k=1}^{m} E\left[\frac{I_F(x)}{h_X(x)} \frac{\partial f_X(x)}{\partial \theta_{x_i}^{(k)}} \alpha_k \right]_{h_X^{(k)}(x)} \tag{26}$$

$$\frac{\partial \hat{P}}{\partial \mu_{x_i}} = \sum_{k=1}^{m} \frac{1}{N_k} \sum_{j=1}^{N_k} \frac{I_F\left(x_j^{(k)}\right) f_X\left(x_j^{(k)}\right) \left(x_{ji}^{(k)} - \mu_{x_i}^{(k)}\right)}{h_X\left(x_j^{(k)}\right) \sigma_{x_i}^{(k)2}} \alpha_k \tag{27}$$

$$\frac{\partial \hat{P}}{\partial \sigma_{x_i}} = \sum_{k=1}^{m} \frac{1}{N_k} \sum_{j=1}^{N_k} \frac{I_F\left(x_j^{(k)}\right) f_X\left(x_j^{(k)}\right)}{\sigma_{x_i}^{(k)} h_X\left(x_j^{(k)}\right)} \left[\frac{\left(x_{ji}^{(k)} - \mu_{x_i}^{(k)}\right)^2}{\sigma_{x_i}^{(k)2}} - 1 \right] \alpha_k \tag{28}$$

where $x_{ji}^{(k)}$ is the i^{th} component belonging to the j^{th} sample of the k^{th} failure mode.

As a result, the reliability and sensitivity analyses from multiple failure modes based on the importance sampling method have both been mentioned. They can both be used for reliability and sensitivity of the machine tool calculation, in order for the error allocation to be presented.

4 Case studies

In order for the proposed error allocation approach based on HTMs and the importance sampling method to be verified, a test was executed on a five-axis machine tool (XKH800). The example consisted of three steps: (1) Laser interferometers were used for the geometric error measurement, and the thermal and cutting force-induced errors were acquired based on G-RBF, in order for the predicted comprehensive errors to be obtained. Following, the programmable machine controller (PMC) of the machine tool gathered the actual comprehensive errors, in order for the comprehensive error model to be verified; (2) a compensation system and the PMC were combined for the thermal and cutting force-induced errors to be compensated, in order for the optimization of the geometric errors based on the reliability and sensitivity analysis to be presented; and

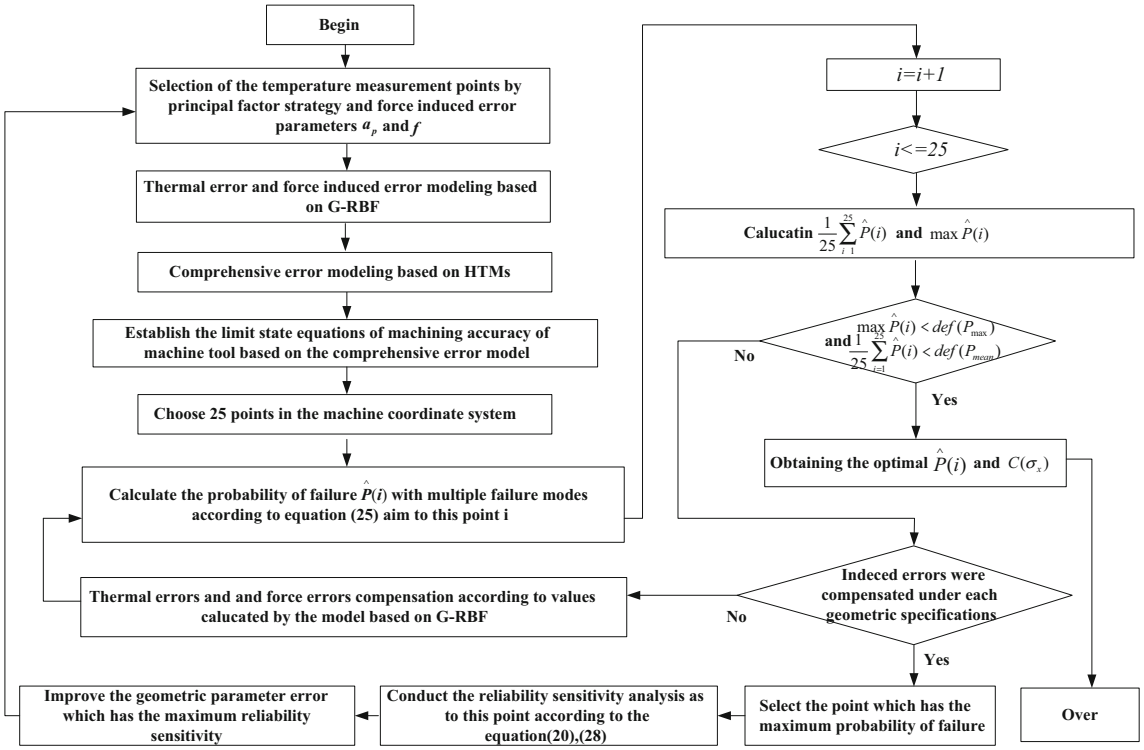

Fig. 8 Flowchart illustrating accuracy allocation

(3) an experiment on the machine tool was used for the optimization result verification.

4.1 The comprehensive error modeling

1. Measurement of the geometric errors

Regarding a comprehensive error model establishment necessity, the geometric errors were measured firstly and various geometric parameter errors had different methods in the measurement process, as follows: (1) The prismatic joint errors (error nos. 1–18 in Table 2) are measured by a laser interferometer (XD6 Standard Laser Measuring System) as shown in Fig. 3a; (2) the rotary joint errors (error nos. 19–30 in Table 2) were measured by a different laser interferometer (Renishaw XL-80) and a mirror as presented in Fig. 3b; and (3) a laser measurement system (Proline V3) was utilized to quantify the squareness errors of prismatic joints (error nos. 37–39), the parallelism errors of rotary joints (error nos.40–43), and the offset errors (error nos. 44–45), as presented in Fig. 3c. Following, the measurement results of the geometric errors are presented in Table 2.

2. Prediction of thermal and cutting force-induced errors

A test for the thermal and cutting force-induced error prediction was conducted on the five-axis NC machine tool, as presented in Fig. 4. Eight temperature measurement points (point 1 to point 8), having larger correlation with the thermal errors produced by preliminary analysis of the structure and working conditions of the machine tool, were selected. During testing, this machine tool machined a leaf for 188 min at typical machining speed in various cutting depths and cutting feeds, as presented in Table 3. An intelligent circuit testing alarming device (KYLC03) was used for the temperature measurement of these eight points simultaneously. A laser interferometer measured the thermal and cutting force-induced errors every 4 min, whereas 48 measurements were conducted in total. Subsequently, the first group of measurement data was collected for the thermal and cutting force-induced error model to be developed. Following this machine tool cooling down to room temperature, the second group of measurement data was collected, in order for the developed model of the thermal and cutting force-induced errors to be verified.

The first group of measurement data, including eight temperature measurement points and two cutting force error parameters, is presented in Fig. 5. The measurement of thermal and cutting force-induced errors of the X-axis, Y-axis, and Z-axis are presented in Fig. 6. The principal factor [35] was used for the temperature measurement point optimization in the paper. Therefore, four temperature measurement points (point 1, point 2, point 3, and point 8) that had the larger correlation with the thermal and force errors were selected.

Regarding the thermal and cutting force-induced error model development, four temperature points, cutting depth a_p, and cutting feed f were used as the input parameters, and the thermal and cutting force-induced errors were used as the output parameters. The fuzzy set of every input parameter

Table 5 Maximum values of geometric parameter errors of the five-axis NC machine tool

Number i	1	2	3	4	5	6	7	8
Parameter	Δx_x	Δy_x	Δz_x	Δa_x	$\Delta \beta_x$	$\Delta \gamma_x$	Δx_y	Δy_y
Value	0.0065 mm	0.0065 mm	0.0065 mm	$\left(\frac{0.0037}{1000}\right)^\circ$	$\left(\frac{0.0037}{1000}\right)^\circ$	$\left(\frac{0.0037}{1000}\right)^\circ$	0.007 mm	0.007 mm
Number i	9	10	11	12	13	14	15	16
Parameter	Δz_y	Δa_y	$\Delta \beta_y$	$\Delta \gamma_y$	Δx_z	Δy_z	Δz_z	$\Delta \alpha_z$
Value	0.007 mm	$\left(\frac{0.0028}{1000}\right)^\circ$	$\left(\frac{0.0028}{1000}\right)^\circ$	$\left(\frac{0.0028}{1000}\right)^\circ$	0.007 mm	0.007 mm	0.007 mm	$\left(\frac{0.0028}{1000}\right)^\circ$
Number i	17	18	19	20	21	22	23	24
Parameter	$\Delta \beta_z$	$\Delta \gamma_z$	Δx_φ	Δy_φ	Δz_φ	$\Delta \alpha_\varphi$	$\Delta \beta_\varphi$	$\Delta \gamma_\varphi$
Value	$\left(\frac{0.0028}{1000}\right)^\circ$	$\left(\frac{0.0028}{1000}\right)^\circ$	0.0058 mm	0.0058 mm	0.0058 mm	$\left(\frac{0.0061}{1000}\right)^\circ$	$\left(\frac{0.0061}{1000}\right)^\circ$	$\left(\frac{0.0061}{1000}\right)^\circ$
Number i	25	26	27	28	29	30	31	32
Parameter	Δx_A	Δy_A	Δz_A	Δa_A	$\Delta \beta_A$	$\Delta \gamma_A$	Δx_B	Δy_B
Value	0.0058 mm	0.0058 mm	0.0058 mm	$\left(\frac{0.0061}{1000}\right)^\circ$	$\left(\frac{0.0061}{1000}\right)^\circ$	$\left(\frac{0.0061}{1000}\right)^\circ$	0.0068 mm	0.0068 mm
Number i	33	34	35	36	37	38	39	40
Parameter	Δz_B	$\Delta \alpha_B$	$\Delta \beta_B$	$\Delta \gamma_B$	$\Delta \gamma_{xy}$	$\Delta \beta_{xz}$	$\Delta \alpha_{yz}$	$\Delta \gamma_{yA}$
Value	0.0068 mm	$\left(\frac{0.0049}{1000}\right)^\circ$	$\left(\frac{0.0049}{1000}\right)^\circ$	$\left(\frac{0.0049}{1000}\right)^\circ$	$\left(\frac{0.0037}{500}\right)^\circ$	$\left(\frac{0.0037}{500}\right)^\circ$	$\left(\frac{0.0037}{500}\right)^\circ$	$\left(\frac{0.011}{300}\right)^\circ$
Number i	41	42	43	44	45			
Parameter	$\Delta \beta_{zA}$	$\Delta \gamma_{xB}$	$\Delta \alpha_{zB}$	Δy_{AB}	Δz_{AB}			
Value	$\left(\frac{0.011}{300}\right)^\circ$	$\left(\frac{0.011}{300}\right)^\circ$	$\left(\frac{0.011}{300}\right)^\circ$	0.0068 mm	0.0068 mm			

Table 6 The initial failure possibility of this machine tool

Vector of point *i*	Monte Carlo	AFOSM		The approach in this paper	
		Possibility of failure	Error%	Possibility of failure	Error%
(40, 40)	0.1158	0.1184	2.245250432	0.1168	0.863557858
(40, 20)	0.0932	0.0976	4.721030043	0.0924	0.858369099
(40, 0)	0.0843	0.0852	1.067615658	0.0845	0.237247924
(40,−20)	0.0932	0.0976	4.721030043	0.0924	0.858369099
(40, −40)	0.1158	0.1184	2.245250432	0.1168	0.863557858
(80, 40)	0.1197	0.1207	0.835421888	0.1189	0.66833751
(80, 20)	0.0932	0.0976	4.721030043	0.0924	0.858369099
(80, 0)	0.0807	0.0809	0.247831475	0.0845	4.708798017
(80, −20)	0.0932	0.0976	4.721030043	0.0924	0.858369099
(80, −40)	0.1197	0.1207	0.835421888	0.1189	0.66833751
(120, 40)	0.1197	0.1207	0.835421888	0.1189	0.66833751
(120, 20)	0.0932	0.0976	4.721030043	0.0924	0.858369099
(120, 0)	0.0861	0.0921	6.968641115	0.0903	4.87804878
(120,−20)	0.0932	0.0976	4.721030043	0.0924	0.858369099
(120, −40)	0.1197	0.1207	0.835421888	0.1189	0.66833751
(160, 40)	0.1204	0.1267	5.23255814	0.123	2.159468439
(160, 20)	0.113	0.1162	2.831858407	0.1107	2.03539823
(160, 0)	0.1041	0.1092	4.899135447	0.1054	1.248799232
(160, −20)	0.113	0.1162	2.831858407	0.1107	2.03539823
(160, −40)	0.1204	0.1267	5.23255814	0.123	2.159468439
(200, 40)	0.1204	0.1267	5.23255814	0.123	2.159468439
(200, 20)	0.113	0.1162	2.831858407	0.1107	2.03539823
(200, 0)	0.1139	0.1158	1.668129939	0.1121	1.580333626
(200, −20)	0.113	0.1162	2.831858407	0.1107	2.03539823
(200, −40)	0.1204	0.1267	5.23255814	0.123	2.159468439
Mean value	0.106892	0.1104	3.33069554	0.107008	1.559334984

contained two fuzzy subsets; therefore, there were 2^6 fuzzy rules in total. The thermal and cutting force-induced error model based on a generalized RBF was developed by Matlab software, and the corresponding predictive ability was validated by the second group of measurement data. Besides, the BP neural network was used for comparison. With the use of the BP network, the number of hidden layer units is generally defined by the $s = \sqrt{m+n} + a$ formula, wherem and n refer to the number of input and output units, respectively, and $a \in [1, 10]$ [37], therefore $m = 6$, $n = 3$, and $a = 5$. The predicted and actual values of the thermal and cutting force-induced errors are presented in Fig. 6. It is clear that residual errors between the predicted and the actual values are significantly small, validating the developed model. Table 4 was acquired according to Fig. 6. It is presented that residual errors of the generalized RBF are clearly smaller than the BP neural network, suggesting that the model based on the generalized RBF has the better predictive ability.

3. The prediction of comprehensive errors.

At present, the comprehensive error model including geometric, thermal, and cutting force-induced errors was developed. Twenty-five points were selected by orthogonal sampling in the working space of the machine tool. Aimed at each point, the predicted values based on the comprehensive error model and the actual machining errors in the X-direction, Y-direction, and Z-direction are presented in Fig. 7, demonstrating that the residual errors between the predicted errors and the actual errors in the X-axis, Y-axis, and Z-axis respectively are small. As a result, the proposed comprehensive error model was verified.

4.2 Optimization of geometric errors

In this paper, an approach for error parameter allocation of a multi-axis NC machine tool based on the importance sampling

Table 7 The failure possibility of this machine tool after thermal and force error compensation

Vector of point *i*	Monte Carlo	AFOSM		The approach in this paper	
		Possibility of failure	Error%	Possibility of failure	Error%
(40, 40)	0.0875	0.0843	3.657142857	0.0892	1.942857143
(40, 20)	0.0682	0.0665	2.492668622	0.0675	1.026392962
(40, 0)	0.0521	0.0495	4.990403071	0.0538	3.262955854
(40, −20)	0.0682	0.0665	2.492668622	0.0675	1.026392962
(40, −40)	0.0875	0.0843	3.657142857	0.0892	1.942857143
(80, 40)	0.0836	0.0828	0.956937799	0.0843	0.837320574
(80, 20)	0.0682	0.0665	2.492668622	0.0675	1.026392962
(80, 0)	0.0621	0.0654	5.314009662	0.063	1.449275362
(80, −20)	0.0682	0.0665	2.492668622	0.0675	1.026392962
(80, −40)	0.0836	0.0828	0.956937799	0.0843	0.837320574
(120, 40)	0.0836	0.0828	0.956937799	0.0843	0.837320574
(120, 20)	0.0682	0.0665	2.492668622	0.0675	1.026392962
(120, 0)	0.0524	0.0533	1.717557252	0.0528	0.763358779
(120, −20)	0.0682	0.0665	2.492668622	0.0675	1.026392962
(120, −40)	0.0836	0.0828	0.956937799	0.0843	0.837320574
(160, 40)	0.0752	0.0703	6.515957447	0.0772	2.659574468
(160, 20)	0.0638	0.0654	2.507836991	0.0644	0.940438871
(160, 0)	0.0522	0.0537	2.873563218	0.0547	4.789272031
(160, −20)	0.0638	0.0654	2.507836991	0.0644	0.940438871
(160, −40)	0.0752	0.0703	6.515957447	0.0772	2.659574468
(200, 40)	0.0752	0.0703	6.515957447	0.0772	2.659574468
(200, 20)	0.0623	0.0652	4.654895666	0.0633	1.605136437
(200, 0)	0.0575	0.0603	4.869565217	0.0582	1.217391304
(200, −20)	0.0623	0.0652	4.654895666	0.0652	4.654895666
(200, −40)	0.0752	0.0703	6.515957447	0.0772	2.659574468
Mean value	0.069916	0.068936	3.450097686	0.070768	1.746192616

method was proposed. This was accomplished by the minimum possibility of failure and cost of machine tools as criterion utilization and the machining accuracy and machine tool reliability selected as constraints. A flowchart of the approach is shown in Fig. 8. Therefore, the effectiveness demonstration of this approach was conducted on a five-axis NC machine tool with a sample.

Based on the comprehensive error model, the expressions with functional specifications of the machine tool, limiting errors in each basic direction, can be formulated as the limit state equations of the machine tool for the reliability and sensitivity of the machine tool to be calculated:

$$\begin{cases} |E_X| \le def(E_X) \\ |E_Y| \le def(E_Y) \\ |E_Z| \le def(E_Z) \end{cases} \tag{29}$$

As forehand mentioned in [2], the five-axis machine tool has 6 single failure modes, 12 double failure modes, and 8 triple failure modes. The design requirements for such a machine tool are the following: The maximum failure probability of the position error being lesser than 0.03 mm should be no more than 5%, and the mean failure probability should not be more than 3%. The values of the geometric parameter errors of the five-axis NC machine tool should not exceed the values shown in Table 5.

During the optimization process, five points (40, 80, 120, 160, 200) on the X-axis and five points (−40, −20, 0, 20, 40) on the Y-axis were chosen by orthogonal sampling for the reliability of this machine tool to be obtained. It is well recognized that the total cost of the machine tool and the corresponding machining accuracy are balanced evenly; therefore, the aim of the optimization process for the multi-axis NC machine tool is the maximum geometric errors σ_{x_i} to be obtained, promising that reliability satisfies the design requirement while optimal total cost is preserved. In the paper, exponential curves have been selected for relationship between the main composing part geometric errors and the manufacturing

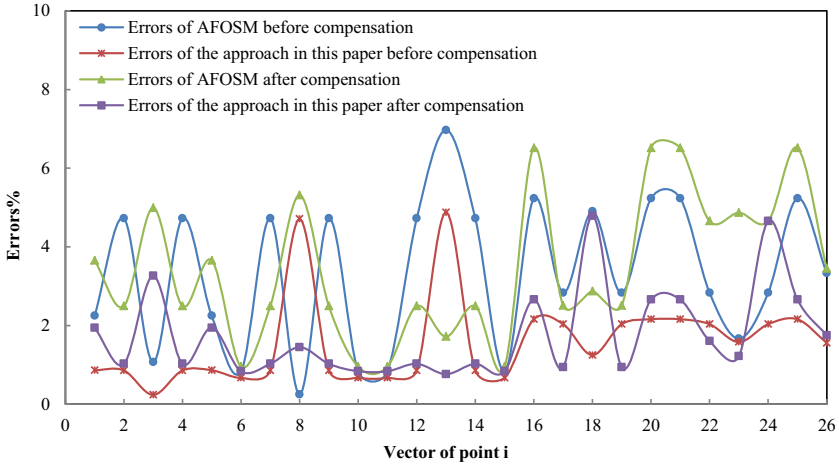

Fig. 9 Comparison of the proposed and alternate method

cost presentation. The typical form for a single geometric error [8] is

$$c(\sigma_{x_i}) = {}_i \cdot e^{-\hbar_i \cdot \sigma_{x_i}} \tag{30}$$

where ${}_i$ and $\hbar_i$ are the constant coefficients and σ_{x_i} is the i^{th} geometric error of a machine tool. For a five-axis machine tool with 45 geometric errors, the total manufacturing cost is resulted to be the sum of the manufacturing cost of each geometric error. This can be expressed as follows:

$$C(\sigma_x) = \sum_{i=1}^{45} c(\sigma_{x_i}) \tag{31}$$

The machining accuracy reliability model for accuracy allocation of the machine tool is given by Eq. (32). The calculation was performed by MatLab software.

$$\begin{aligned} M: \quad & \min \hat{P}(i), \min C(\sigma_x) \\ S.t.: \quad & 0 < \sigma_{x_i} \le def(\sigma_{x_i}) \\ & \frac{1}{25}\sum_{i=1}^{25} \hat{P}(i) \le 3\% \\ & \max \hat{P}(i) \le 5\% \end{aligned} \tag{32}$$

Firstly, the $\max P^{\wedge}(i)$ including the geometric, thermal, and cutting force-induced errors were obtained. According to constraint conditions, if $\max P^{\wedge}(i) > 5\%$ or $\frac{1}{25}\sum_{i=1}^{25} \hat{P}(i) > 3\%$, a compensation system, being independent from the machine tool, was used to compensate the thermal and cutting force-induced errors. It was developed based on the proposed thermal and cutting force-induced error model and the compensation process as follows: (1) The temperatures were acquired from four temperature sensors, the machining parameters were defined beforehand, and the actual positions were obtained by the programmable machine controller (PMC) of the machine tool, respectively. Following, the parameters were inserted into the thermal and cutting force-induced error model of the compensation system for real-time error compensated values to be predicted. (2) The compensation system sends the messages to the PMC after one PMC scanning period, which includes adding the compensation trigger signal, the axis to be compensated, and the compensation values of the specified address. (3) The PMC of the machine tool conducted the error real-time compensation, and the next cycle of the error compensation begins. Accepting that

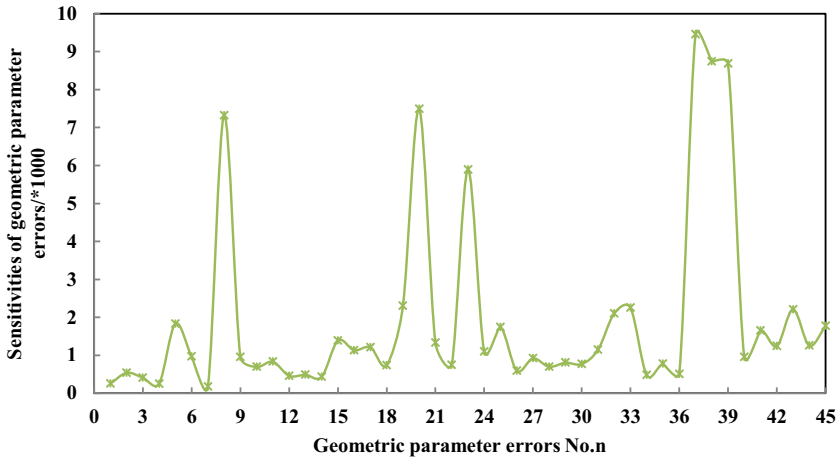

Fig. 10 Results of the machining accuracy sensitivity analysis

Table 8 Reliability of each improvement after thermal and force error compensation

	Δy_y	Δy_φ	$\Delta\beta_\varphi$	$\Delta\gamma_{xy}$	$\Delta\beta_{xz}$	$\Delta\alpha_{yz}$	Possibility of failure		Cost
							Max	Mean	
Before improvement	0.0064	0.0053	0.0058/1000	0.0034/500	0.0034/500	0.0034/500	8.92%	7.08%	116.54
Improvement no. 1	0.0061	0.005	0.0055/1000	0.0031/500	0.0031/500	0.0031/500	6.89%	5.26%	157.62
Improvement no. 2	0.0058	0.0047	0.0052/1000	0.0028/500	0.0028/500	0.0028/500	5.15%	3.97%	226.13
Improvement no. 3	0.0055	0.0044	0.0049/1000	0.0025/500	0.0025/500	0.0025/500	4.33%	2.74%	312.75
Improvement no. 4	0.0052	0.0041	0.0046/1000	0.0022/500	0.0022/500	0.0022/500	3.32%	1.93%	492.30
Improvement no. 5	0.0049	0.0038	0.0043/1000	0.0019/500	0.0019/500	0.0019/500	2.82%	1.41%	784.18

the residual errors based on the generalized RBF are quite small, an assumption can be made that the predicted values for the thermal and cutting force-induced errors are equal to the actual values. As a result, the max $P^{\wedge}(i)$ including only the geometric errors was obtained. If $\max P^{\wedge}(i) > 5\%$ or $\frac{1}{25}\sum_{i=1}^{25} \hat{P}(i) > 3\%$, then $\max P^{\wedge}(i)$ was chosen for $\frac{\partial \max \partial P^{\wedge}(i)}{\partial \sigma_{x_i}}$ to be calculated leading to geometric error determination improvement. Following each improvement, the thermal and force-induced errors should be recalculated by thermal error modeling method usage, based on a generalized RBF. This process would be over until $\max P^{\wedge}(i) \leq 5\%$ and $\frac{1}{25}\sum_{i=1}^{25} \hat{P}(i) > 3\%$. Therefore, $\min C(\sigma_x)$ is obtained. During optimization, the cost of each improvement is corresponding to the values of all geometric parameter errors σ_{x_i} of each improvement. In this expression, σ_{x_i} should not exceed the initial values presented in Table 5. The common calculation methods, such as Monte Carlo and the advanced first-order and second-moment (AFOSM), were used for verification and comparison. The values of failure possibility of machining accuracy, before and after compensation of the thermal and force errors without any improvement in geometric errors, were acquired according to different reliability analysis methods, presented in Tables 6 and 7. Figure 9 is acquired from Tables 6 and 7 and demonstrates that the approach errors in this paper were no more than the errors of the AFOSM, when Monte Carlo was considered as a reference. Therefore, the proposed approach has higher precision.

Tables 6 and 7 present the maximum (11.89 and 8.92%) and the mean (10.7 and 7.08%) values of the failure possibility before any improvement exceeded the required values (5 and 3%), suggesting that current levels of the geometric errors fail to meet the design requirement. Therefore, it is necessary for a reliability sensitivity analysis to be conducted in order for the geometric errors of machine tools to be optimized. The results of the sensitivity analysis are presented in Fig. 10, configuring all 45 geometric errors with the number in Table 4 as the X-axis and the sensitivity of each geometric error as the Y-axis. From Fig. 10, it can be discovered that the geometric errors Δy_y, Δy_A, $\Delta\beta_A$, $\Delta\gamma_{xy}$, $\Delta\beta_{xz}$, and $\Delta\alpha_{yz}$ have the larger effect on the failure possibility, consequently being the improved objects. The failure possibility and cost of the machine tool, corresponding to the geometric errors of each improvement, are presented in Table 8.

From Fig. 11, it can be noticed that as geometric errors were improved, the tendency of the failure possibility of the machine tool decreases and the cost of the machine tool

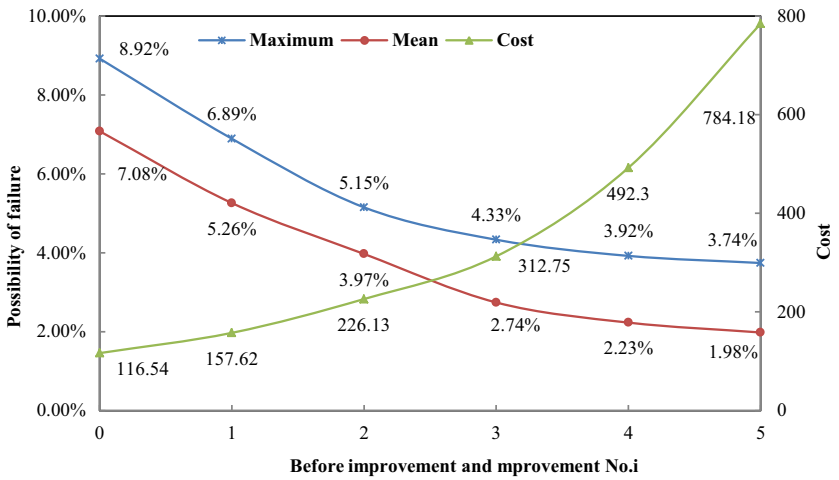

Fig. 11 The tendency of the failure possibility and the cost of each improvement

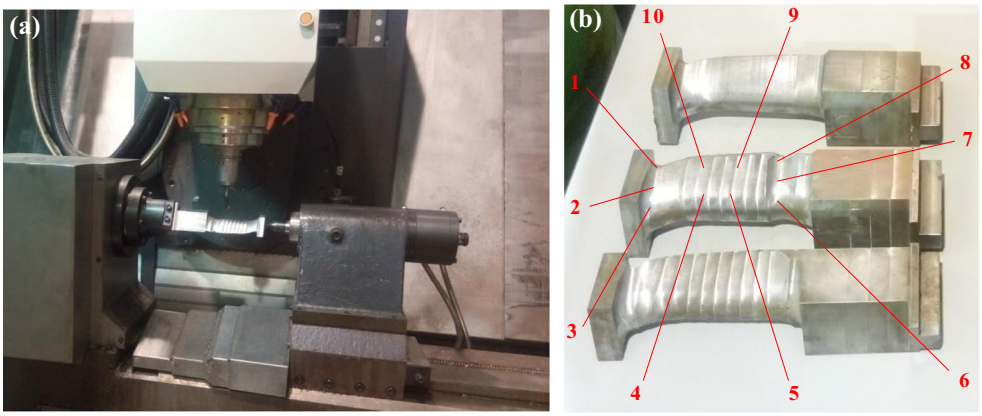

Fig 12 The machining process and the workpieces of the machine tool

projected a rise tendency. When the improved levels of these six geometric errors are not too high (before the forth improvement), the maximum and mean failure possibility decreases straightly and the cost increases moderately. However, as the improved levels of these six geometric errors rise (the fifth improvement), the maximum and mean possibility of failure decreases a little and the cost rises straightly. Regarding machine tool builders, specifications and cost of machine tools are two antagonistic aspects that should be considered simultaneously. Therefore, there is no need for a machine tool with the highest specifications to be designed, whereas for the cost of the machine tool, a straight rise must occur while the reliability of the machine tool does not show a similar rise if geometric errors are allocated within the rather higher levels. As a result, the optimal improvement is the third improvement that ensures reliability, meeting the design requirements with an optimum cost.

4.3 Verification of the optimization results

Concerning the effectiveness of the optimization result verification, an actual experiment was performed on the remanufactured five-axis machining center (XKH800) able to process different materials and shapes. It has processed the blades made by 45#, continuously for 40 weeks including two periods: 1–20th weeks (before optimization) and 21–40th weeks (after optimization). During the experiment as shown in Fig. 12a, the machining count was four every day, and as a result, the test number of each vector for each period was 560. As presented in Fig. 12b, ten points of each workpiece were used for the measurement and the failure number of each point recorded to calculate the failure possibility, and the results of the experiment are presented in Table 9. From Table 9, it can be observed that before optimization, the maximum failure possibility was 8.75% and the mean failure possibility was 6.91% and an excess of 5 and 3% occurred, failing to meet the design requirements of the machine tool. However, following optimization of the geometric parameter errors, the maximum failure possibility was 4.11% and the mean failure possibility was 2.79%, both being below 5 and 3%, suggesting that reliability improved and design requirement was met. As a result, the accuracy design approach was proposed in the

Table 9 Results of failure possibility before and after optimization

Point *i*	Test number	Before optimization		After optimization	
		Failure number	Failure possibility	Failure number	Failure possibility
1	560	49	8.75%	23	4.11%
2		36	6.43%	16	2.86%
3		46	8.21%	22	3.93%
4		36	6.43%	10	1.79%
5		33	5.89%	9	1.61%
6		45	8.04%	22	3.93%
7		37	6.61%	15	2.68%
8		42	7.50%	20	3.57%
9		34	6.07%	9	1.61%
10		29	5.18%	10	1.79%
Mean value	560	38.7	6.91%	15.6	2.79%

paper and the optimal results were verified by the experiment.

5 Conclusions

Geometric, thermal, and cutting force-induced errors contribute to the machining accuracy of an NC machine tool, significantly. Therefore, the forehand mentioned induced errors constitute an important role for the permissible level of each error parameter determination of a machine tool. In this paper, a general approach that simultaneously considered all three kinds of errors, aiming to the accuracy design performance of machine tools, was proposed. It consists of the following steps:

1. A thermal and cutting force-induced error model of an NC machine tool was developed, based on a generalized (RBF) neural network. Following, a comprehensive error model explaining how various errors affected the machining accuracy was obtained, through HTM usage.
2. Based on this comprehensive error model and the importance sampling method, a reliability model for reliability prediction of this machine tool and a reliability sensitivity model for identification and optimization of error parameters that affected reliability significantly were presented.
3. The proposed approach was applied to a five-axis machine tool and verified by an experiment, meaning that it is possible for the error allocation of a machine tool to be presented, while the total cost is retained optimized.

Despite the forehand mentioned progress, two issues can be investigated further for future improvements:

1. The proposed thermal and force-induced error models consider only the spindle; however, the thermal and force-induced errors of other parts and components such as the guide and the ball screw also affected the machining accuracy.
2. During machining, all errors were characteristic of time variation, causing the reliability of a machine tool to change as time passes.

Therefore, the development of an accuracy design approach for NC machine tools based on reliability theory, while the forehand mentioned two points are considered, will be of focus for future research.

Acknowledgements The authors are very grateful to the National Natural Science Foundation of China (51575009), the Jing-Hua Talents Project of Beijing University of Technology, the National Science and Technology Major Project (2014ZX04010-011), the National Natural Science Foundation of China (51575010), Beijing Nova Program (Z151100003150138), the Leading Talent Project of Guangdong Province, Open Project of State Key Lab of Digital Manufacturing Equipment & Technology (Huazhong University of Science and Technology), Shantou Light Industry Equipment Research Institute of Science and Technology Correspondent Station (2013B090900008), and the National Science and Technology Major Project (2013ZX04013-011) for supporting the research presented in this paper.

References

1. Cai LG, Zhang ZL, Cheng Q, Liu ZF, Gu PH (2015) A geometric accuracy design method of multi-axis NC machine tool for improving machining accuracy reliability. Eksploatacja i Niezawodnosc-Maintenance and Reliability 17(1):143–155
2. Cai LG, Zhang ZL, Cheng Q, Liu ZF, Gu PH, Qi Y (2016) An approach to optimize the machining accuracy retainability of multi-axis NC machine tool based on robust design. Int. J. Precis Eng 43: 370–386
3. António CC, Hoffbauer LN (2009) An approach for reliability-based robust design optimisation of angle-ply composites. Compos Struct 90:53–59
4. Chen ZJ (2008) Real-time compensation of cutting forces induced error on CNC machine tools. Dissertation, Shanghai Jiao Tong University
5. Cheng Q, Feng QN, Liu ZF, Gu PH, Zhang GJ (2016) Sensitivity analysis of machining accuracy of multi-axis machine tool based on POE screw theory and Morris method. Int J Adv Manuf Technol 84(9–12):2301–2318
6. Cheng Q, Qi Z, Zhang GJ, Zhao YS, Sun BW, Gu PH (2015) Robust modeling and prediction of thermally induced positional error based on grey rough set theory and neural network. Int J Adv Manuf Technol 83(5–8):753–764
7. Cheng Q, Zhao HW, Zhang GJ, Gu PH, Cai LG (2014) An analytical approach for crucial geometric errors identification of multi-axis machine tool based on global sensitivity analysis. Int J Adv Manuf Technol 75(1–4):107–121
8. Choi JH, Lee WH, Park JJ, Youn BD (2008) A study on robust design optimization of layered plate bonding process considering uncertainties. Struct Multidiscip Optim 35:531–540
9. Dong Z, Hu W, Xue D (1994) New production cost-tolerance models for tolerance synthesis. ASME J Eng Ind 116:199–206
10. Dorndorf U, Kiridena VSB, Ferreira PM (1994) Optimal budgeting of quasistatic machine tool errors. J Eng Ind 116(1):42–53
11. Dufour P, Groppetti R. (2006) Computer aided accuracy improvement in large NC machine-tools. In Proceedings of the 2006 International Conference on the MTDR 22: 611–618.
12. Fu GQ, Fu JZ, Shen HY, Xu YT, Jin Y (2015) Product-of-exponential formulas for precision enhancement of five-axis machine tools via geometric error modeling and compensation. Int J Adv Manuf Technol 81(1–4):289–305
13. Fu GQ, Fu JZ, Xu YT, Chen ZC (2014) Product of exponential model for geometric error integration of multi-axis machine tools. Int J Adv Manuf Technol 71(9–12):1653–1166
14. Geng JH (2015) Research on error modeling of cutting force and analysis and application of threedimensional heat critical point of CNC machine tools. Dissertation, Anhui University of Science and Technology
15. Guo QJ, Yang JG, Wu H (2010) Application of ACO-BPN to thermal error modeling of NCmachine tool. Int J Adv Manuf Technol 50:667–675
16. Hocken RJ, Simpson JA, Borchardt B, Lazar J, Reeve C, Stein P (1977) Three dimensional metrology. Journal of Ann. CIRP 26(2): 403–408

17. Huang X, Ding W, Hong R (2006) Research on accuracy design for remanufactured machine tools. In Proceedings of the 2006 International Conference on Technology and Innovation 1403–1410
18. Krishna AG, Rao KM (2006) Simultaneous optimal selection of design and manufacturing tolerances with different stack-up conditions using scatter search. Int J Adv Manuf Technol 30(3–4):328–333
19. Kiridena V, Ferreira PM (1993) Mapping the effects of positioning errors on the volumetric accuracy of five-axis CNC machine tools. Int J Mach Tools Manuf 33(3):417–437
20. Jin S, Zheng C, Yu K, Lai X (2010) Tolerance design optimization on cost-quality trade-off using the Shapley value method. J Manuf Syst 29(4):142–150
21. Li SY, Dai YF, Yin ZQ, Zheng ZW, Wang GL, Peng ZQ (2007) Accuracy modeling technology of precision and ultra-precision machine tool. National University of Defense Technology Press, Changsha
22. Liu H, Li B, Wang X, Tan G (2011) Characteristics of and measurement methods for geometric errors in CNC machine tools. Int J Adv Manuf Technol 54(1–4):195–201
23. Liu YW, Zhang Q, Zhao XS, Zhang ZF (2002) Multi-body system based technique for compensating thermal errors in machining centers. Chin J Mech Eng 38(1):127–130
24. Lu ZY, Song SF, Li HS, Yuan XK (2009) Structural reliability and reliability sensitivity analysis organization. Sciences Press, Beijing
25. Lv C, Liu ZY, Liu ZJ, Yu ZM (2015) Application of generalized radial basis function neural network to thermal error modeling. Opt Precis Eng 23(6):1705–1713
26. Portman VT (1982) A universal method for calculating the accuracy of mechanical devices. J Sov Eng Res 1(7):11–15
27. Raksiri C, Parnichkun M (2004) Geometric and force errors compensation in a 3-axis CNC milling machine. Int J Mach Tools Manuf 44(12/13):1283–1291
28. She CS, Huang ZH (2008) Postprocessor development of a five-axis machine tool with mutating head and table configuration. Int J Adv Manuf Technol 38(7):728–740
29. Shi XL, Liu HL, Li H, Liu C, Tan GY (2016) Comprehensive error measurement and compensation method for equivalent cutting forces. Int J Adv Manuf Technol 85(1–4):149–156
30. Shi YG, Zhao XY, Zhang HJ, Nie YX, Zhang DW (2016) A new top-down design method for the stiffness of precision machine tools. Int J Adv Manuf Technol 83(9–12):1887–1904
31. Wang HT, Wang LP, Li TM, Han J (2013) Thermal sensor selection for the thermal error modeling of machine tool based on the fuzzy clustering method. Int J Adv Manuf Technol 69:121–126
32. Wang SX, Yun JT, Zhang ZF (2003) Modeling and compensation technique for the geometric errors of five-axis CNC machine tools. Chin J Mech Eng 16(2):197–201
33. Wu H, Jiliweisi ZHT, Yang JG (2005) Cutting force error modeling of NC machine tool and real-time compensation based on the current measurement. Chin J Mech Manuf 43(492):13–15
34. Wu H, Yang JG, Zhao HT (2008) Synthetically modeling for the thermal error and cutting force induced error on a CNC Turning Center. J Sichuan Univ (Engineering science edition) 40(2):165–169
35. Yang JG, Wang XS, Zhao HT (2005) Temperature measurement points optimization selection of machine tools. Chinese Mechanical Engineering Society annual conference 627–632
36. Yu ZM, Liu ZJ, Ai YD, Xiong M (2013) Geometric error model and precision distribution based on reliability theory for large CNC gantry guideway grinder. Chin J Mech Eng 49(17):142–151
37. Zhang Y, Yang JG, Jiang H (2012) Machine tool thermal error modeling and prediction by grey neural network. Int J Adv Manuf Technol 59:1065–1072
38. Zou HB, Chen XD, Wang SJ (2015) A study of single kinematic errors accurate fitting for ultra-precision micro v-groove machine tools. Int J Adv Manuf Technol 77(5–8):1345–1351